

DreamMapping: High-Fidelity Text-to-3D Generation via Variational Distribution Mapping

Zeyu Cai^{1*} , Duotun Wang^{1,3*} , Yixun Liang¹ , Zhijing Shao¹ , Ying-Cong Chen^{1,2} , Xiaohang Zhan³ , and Zeyu Wang^{1,2} 

¹The Hong Kong University of Science and Technology (Guangzhou)

²The Hong Kong University of Science and Technology

³Tencent AI Lab



Figure 1: Examples of diverse 3D content generated by DreamMapping given text input. Our framework facilitates the rapid distillation of high-fidelity appearance and geometry from pre-trained 2D diffusion models in a short optimization time (~ 15 mins on a single A100 GPU).

Abstract

Score Distillation Sampling (SDS) has emerged as a prevalent technique for text-to-3D generation, enabling 3D content creation by distilling view-dependent information from text-to-2D guidance. However, they frequently exhibit shortcomings such as over-saturated color and excess smoothness. In this paper, we conduct a thorough analysis of SDS and refine its formulation, finding that the core design is to model the distribution of rendered images. Following this insight, we introduce a novel strategy called Variational Distribution Mapping (VDM), which expedites the distribution modeling process by regarding the rendered images as instances of degradation from diffusion-based generation. This special design enables the efficient training of variational distribution by skipping the calculations of the Jacobians in the diffusion U-Net. We also introduce timestep-dependent Distribution Coefficient Annealing (DCA) to further improve distilling precision. Leveraging VDM and DCA, we use Gaussian Splatting as the 3D representation and build a text-to-3D generation framework. Extensive experiments and evaluations demonstrate the capability of VDM and DCA to generate high-fidelity and realistic assets with optimization efficiency.

CCS Concepts

• Computing methodologies \rightarrow Image manipulation; Shape modeling;

1. Introduction

There has been an increasing need for digital 3D assets in video games [ZW12], mixed reality storytelling [CT14, HWW*21], and digital fabrications [Ger12]. However, this widespread growth highlights the need for more efficient 3D content creation, as crafting 3D assets in graphics software is often time-consuming and labor-intensive. Thanks to the rapid development of diffusion models [HJA20, DN24], recent text-to-3D techniques offer a more accessible and efficient solution for controllable 3D content creation.

Based on the pre-trained text-to-image models [RBL*22, SME21], Score Distillation Sampling (SDS) [PBJM23, WDL*23] provides pixel-level guidance of 3D assets optimization and has become quite effective and popular for text-to-3D generation. Follow-up works further refine the supervision loss and optimization procedures to produce more realistic and semantic-aligned 3D models [WLW*23, CCH*23, CCJJ23, YGL*23, KPCOL24, WZY*24, LSS24, AKS24, WZSZ23, LYL*23, TWWZ23, YCC*23].

In this paper, we review SDS-based 3D generation and its variations, leading to a unifying goal across previous work on refining SDS formulation: establishing a variational distribution for rendered images. Our review and analysis demonstrate that prior efforts have predominantly adopted one of two strategies: 1) utilizing unmodified diffusion models to approximate the variational distribution [YGL*23, KPCOL24, LYL*23, WZY*24] with improved loss designs, and 2) constructing the variational distribution directly through fine-tuning diffusion models [WLW*23, LSS24, WZSZ23, YCC*23] or pre-training a bespoke model [AKS24]. However, the former approach struggles to represent the distribution accurately, since the rendered images during the optimization process are out-of-domain (OOD) cases as to diffusion models [KPCOL24]. Meanwhile, the latter choice demands substantial resources and may exhibit instability during optimization.

To address these issues, we propose variational distribution mapping (VDM), a novel method treating rendered images as a degraded form of images generated by the diffusion model. VDM efficiently formulates the variational distribution of rendered images by modeling and optimizing the degradation process (i.e., lightweight trainable neural network), which enables us to establish a distribution mapping between the generated and the rendered image distributions (Figure 2). Compared with previous methods, VDM has two notable advantages: 1) By introducing the trainable degradation process, it eliminates the need for the complex Jacobian matrix calculations in the UNet of diffusion model, unlike previous variational distribution modeling approaches [WZSZ23, YCC*23]; 2) VDM dynamically models the variational distribution of rendered images, surpassing methods that rely on an unmodified diffusion model with extra batch processing [KPCOL24, YGL*23] for distribution estimation, thereby enhancing generation quality.

Additionally, we analyze the mode-seeking behavior in SDS and further investigate the probabilistic correlation between the distributions of generated and rendered images. We find that the interdependence of their distributions diminishes as the timestep t decreases. This observation motivates the introduction of the distribution coefficient annealing (DCA) strategy. It applies a time-dependent coefficient to accommodate the dynamic changes of rendered image distribution, thereby improving the generation quality.

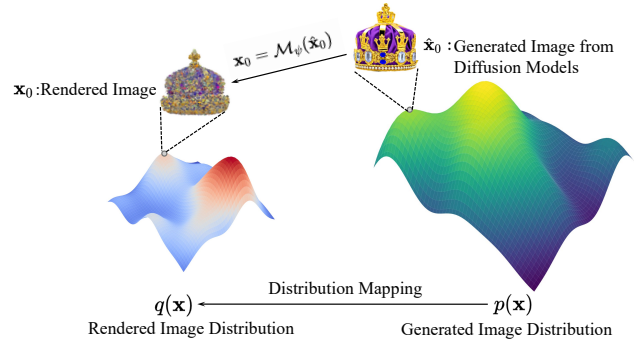


Figure 2: Illustration of our degradation design on the image distributions. We propose the rendered image \mathbf{x}_0 can be degraded from the generated image $\hat{\mathbf{x}}_0$ using the trainable degradation operator \mathcal{M}_ϕ . During SDS optimization, \mathcal{M}_ϕ can efficiently map the image distributions from $p(\mathbf{x})$ to $q(\mathbf{x})$. Detailed discussions are in Sec. 4.2.

To demonstrate the generation ability of our proposed methods, we develop a text-to-3D framework incorporating Shap-E [JN23] for initialization and 3D Gaussian Splatting [KKLD23] as the 3D representation. We present three key contributions as follows:

- We systematically review recent SDS-based methods and reveal their limitations, e.g., limited accuracy and efficiency in constructing variational distributions.
- We introduce VDM and the accompanying DCA strategy, which conceptualizes rendered images as degraded diffusion model outputs for rapid variational distribution constructions. Our approach facilitates creating detailed, realistic 3D assets at a reasonable Classifier Free Guidance (CFG) scale [HS21], i.e., 7.5.
- With VDM and DCA, we develop a novel text-to-3D generative framework using Gaussian Splatting, which outperforms existing methods, as demonstrated through extensive evaluations.

2. Related Work

2.1. Text-to-3D Generation

With the rapid advancement of diffusion models and 3D representations, significant progress has been made in text-based generation. DreamFields [JMB*22] introduced the optimization of Neural Radiance Fields (NeRF) using guidance from pre-trained CLIP models, but the quality was limited due to the CLIP loss’s insufficient semantic guidance. Building on this, DreamFusion [PBJM23] and SJC [WDL*23] developed SDS, a novel loss function based on probability density distillation that provides pixel-level guidance by seeking specific modes in a text-guide diffusion model, enhancing the quality and efficiency of optimization-based 3D generation.

The advent of SDS marked a turning point that inspired a series of subsequent works in 3D generation [WLW*23, YGL*23, KPCOL24, LSS24, LYL*23, YCC*23, WZSZ23]. These studies have refined the generation of 3D assets from various perspectives. Some utilizes advanced differentiable 3D representations to enhance outcomes [LGT*23, CCJJ23], while others [WZY*24] focus

on mitigating the ‘‘Janus’’ problem [HAK23, AKS24]. Zero-1-to-3 [LWH*23] and MVDream [SWY*24] fine-tuned the diffusion model with multi-view image datasets to improve 3D consistency. Perp-Neg [ASZ*23] alleviates the Janus problem with view-dependent negative prompts, and ESD [WXF*23] introduces a view-conditioned loss to improve multi-view generation.

A central emphasis in recent research lies in refining the original SDS methodology, aiming to secure more precise guidance from diffusion models. ProlificDreamer [WLW*23] introduces a Variational Score Distillation Sampling technique to alleviate the mode collapse issue inherent to SDS. To further mitigate over-saturation and over-smoothness problems, TextMesh [TMT*24] enforces textured optimizations with high SDS gradients only and integrates multi-view consistent diffusion. Make-it-3D [TWZ*23] proposes two-stage optimizations to enhance textured appearance; Fantasia3D [CCJJ23] dynamically adjusts the time-dependent weighting function in SDS computations. Meanwhile, CSD [YGL*23] and NFSD [KPCOL24] demonstrate the pivotal role of the conditional term in SDS for 3D generation. They employ additional negative prompts to refine the optimization process. Their explorations highly inspired our work, and we propose further improving SDS with the trainable construction of variational distribution. We will continue more in-depth discussions in Sec. 4.1.

2.2. Differentiable 3D Representations

The differentiable 3D representations are pivotal to text-to-3D generation. A 3D model parameterized by θ is rendered into an image from camera viewpoint c using the differentiable rendering function $g(\theta, c)$. This allows for optimizing the 3D models through backpropagation to align with pixel-level guidance derived from diffusion models. Numerous differentiable 3D representations have been utilized in prior text-to-3D works [PJB23, LGT*23, MRP*22, GAG*23, TRZ*23], including NeRF [MST*20] which is frequently employed in generation tasks. However, NeRF’s volume rendering is computationally intensive, posing challenges for rendering high-resolution images efficiently enough to leverage the diffusion model’s guidance.

To mitigate this constraint, DMTet [SGY*21] has been introduced to integrate both explicit and implicit representations, which has gained increasing utilizations [CCJJ23, LWW*23]. Additionally, there is a growing interest in applying purely explicit representations to facilitate smooth shape manipulations within graphics software. This involves a gradient-based mesh deformation approach to create 3D models [GAG*23, WMC*24]. Notably, 3D Gaussian Splatting [KKLD23] has emerged as an efficient and high-quality explicit representation for reconstruction tasks and has been incorporated into several text-to-3D generation works [TRZ*23, YFW*24, LYL*23]. We investigate Gaussian Splatting as the 3D representation for our generation framework.

3. Preliminaries

In this section, we briefly introduce diffusion models and SDS, which are the fundamental theories of this work.

3.1. Diffusion Models

The Diffusion Model [HJA20, SME21, LYB*24] is a likelihood-based generative model designed to approximate the data distribution p_{data} starting from gaussian noise. Given a sample \mathbf{x} from p_{data} , the model undergoes a forward diffusion process over a series of timesteps $t \in [0, t_{max}]$, whereby noise is incrementally added to transform \mathbf{x} into Gaussian noise $\mathbf{x}_T \sim \mathcal{N}(0, I)$. The diffusion at each step is described by:

$$p(\mathbf{x}_t | \mathbf{x}_{t-1}) = \mathcal{N}(\mathbf{x}_t; \sqrt{1 - \beta_t} \mathbf{x}_{t-1}, \beta_t I), \quad (1)$$

where β_t is a predetermined noise schedule and $\mathbf{x}_0 = \mathbf{x} \sim p_{data}$. To reverse this process, a learnable UNet [RFB15] with parameters ϕ estimates the posterior:

$$p_\phi(\mathbf{x}_{t-1} | \mathbf{x}_t) = \mathcal{N}(\mathbf{x}_{t-1}; \sqrt{\bar{\alpha}_{t-1}} \mu_\phi(\mathbf{x}_t), (1 - \bar{\alpha}_{t-1}) \Sigma_\phi(\mathbf{x}_t)), \quad (2)$$

with $\mu_\phi(\mathbf{x}_t)$ and $\Sigma_\phi(\mathbf{x}_t)$ representing the mean and variance predictions for \mathbf{x}_t , and $\bar{\alpha}_t := \prod_1^t (1 - \beta_t)$.

The training goal is to optimize $\mu_\phi(\mathbf{x}_t)$ and $\Sigma_\phi(\mathbf{x}_t)$ to maximize the log likelihood’s variational lower bound. In practice, the learning target is re-parameterized to the added noise $\epsilon \sim \mathcal{N}(0, I)$ which is used to produce \mathbf{x}_t from $\mathbf{x} = \mathbf{x}_0$, and the notation of UNet in diffusion models is $\epsilon_\phi(\mathbf{x}_t, t)$. The learning process of diffusion models can be interpreted as predicting the noise ϵ that corrupts the data \mathbf{x} . Furthermore, recent studies [LYB*24, SE19] have shown that $\epsilon_\phi(\mathbf{x}_t, t)$ corresponds to the score function $\nabla_{\mathbf{x}_t} \log p_\phi(\mathbf{x}_t)$, indicating the model’s ability to guide \mathbf{x}_t towards regions of higher density within $p_\phi(\mathbf{x}_t)$, which can be approximated as:

$$\nabla_{\mathbf{x}_t} \log p_\phi(\mathbf{x}_t) \approx -\frac{1}{\sqrt{1 - \bar{\alpha}_t}} \epsilon_\phi(\mathbf{x}_t, t). \quad (3)$$

Classifier Free Guidance: Compared with unconditional image generation, text-guided image generation [HS21, SCS*22, RBL*22] has a higher demand. Conditioned on the text prompt y , diffusion models accept it as another input for the diffusion process, denoted as $\epsilon_\phi(\mathbf{x}_t, t, y)$, with related score function $\nabla_{\mathbf{x}_t} \log p(\mathbf{x}_t | y)$. Classifier Free Guidance (CFG) [HS21] is utilized as an implicit classifier to get the textual guidance for image generation. It has a changeable hyperparameter named CFG scale, hereafter denoted as s , and the original prediction is changed as:

$$\epsilon_\phi^{\text{CFG}}(\mathbf{x}_t, t, y) = \epsilon_\phi(\mathbf{x}_t, t, y) + s \cdot (\epsilon_\phi(\mathbf{x}_t, t, y) - \epsilon_\phi(\mathbf{x}_t, t)). \quad (4)$$

As mentioned in Eq. (3), this prediction is also related to a corresponding score function using Bayes’ rule:

$$\epsilon_\phi^{\text{CFG}}(\mathbf{x}_t, t, y) \propto \nabla_{\mathbf{x}_t} \log p_\phi(\mathbf{x}_t | y) + s \cdot \nabla_{\mathbf{x}_t} \log p_\phi(y | \mathbf{x}_t). \quad (5)$$

the latter term can be intuitively understood as guiding x_t being more in line with the text description y .

3.2. SDS with Differentiable Rendering

As demonstrated in Sec. 2.1, SDS [PJB23, WDL*23] is an optimization-driven 3D generative technique that leverages pre-trained 2D diffusion models. Let $\mathbf{x}_0 = g(\theta, c)$ represent the rendered image derived from differentiable 3D representations, parameterized by θ and camera pose c . The distribution of noisy rendered

images is then formulated as follows:

$$q^\theta(\mathbf{x}_t) = \mathcal{N}(\mathbf{x}_t; \sqrt{\bar{\alpha}_t}\mathbf{x}_0, (1 - \bar{\alpha}_t)I). \quad (6)$$

SDS adopts text-conditioned noisy real image distribution $p_\phi(\mathbf{x}_t|y)$ represented by pre-trained Stable Diffusion [RBL*22] and optimizes the parameter θ by minimizing the following KL divergence for all timestep t :

$$\min_{\theta \in \Theta} \mathcal{L}_{SDS}(\theta) := \mathbb{E}_{t,c} \left[\omega(t) D_{KL}(q^\theta(\mathbf{x}_t) || p_\phi(\mathbf{x}_t|y)) \right], \quad (7)$$

where $\omega(t)$ is a time-dependent weighting function. Eq. (7) can be further rewritten as the gradient of a weighted probability density distillation loss to update θ :

$$\nabla_\theta \mathcal{L}_{SDS}(\theta) \approx \mathbb{E}_{t,\epsilon,c} [\omega(t) (\epsilon_\phi(\mathbf{x}_t, t, y) - \epsilon) \frac{\partial \mathbf{x}}{\partial \theta}], \quad (8)$$

where $\epsilon \sim \mathcal{N}(0, I)$ and the UNet Jacobian term $\frac{\partial \epsilon_\phi(\mathbf{x}_t, t, y)}{\partial \mathbf{x}}$ is ignored based on the analysis in DreamFusion [PJBM23].

4. Methodology

4.1. Systematic Review of Advancements in SDS

As outlined in Sec. 3.2, SDS employs a formal gradient, detailed in Eq. (8), to optimize the 3D representation during generation. To achieve text-guided 3D generation, SDS integrates textual information through the common CFG form, as shown in Eq. (4). Consequently, the practical SDS gradient expression is:

$$\nabla_\theta \mathcal{L}_{SDS}(\theta) = \mathbb{E}_{t,\epsilon,c} [\omega(t) (\epsilon_\phi^{CFG}(\mathbf{x}_t, t, y) - \epsilon) \frac{\partial \mathbf{x}}{\partial \theta}], \quad (9)$$

and the noise residual can be further formed as:

$$\epsilon_\phi^{CFG}(\mathbf{x}_t, t, y) - \epsilon = \underbrace{\epsilon_\phi(\mathbf{x}_t, t, y) - \epsilon}_{\text{unconditional term}} + \underbrace{s \cdot (\epsilon_\phi(\mathbf{x}_t, t, y) - \epsilon_\phi(\mathbf{x}_t, t))}_{\text{conditional term}}, \quad (10)$$

which delineates two components: the unconditional and the conditional terms. Numerous studies have indicated that the conditional term pivotal in ensuring the rendered image aligns with textual semantics [WLW*23, YGL*23, KPCOL24, TWWZ23]. This term is further guided by the score function $\nabla_{\mathbf{x}} \log p_\phi(y|\mathbf{x}_t)$, as indicated in Eq. (5). Consequently, subsequent research mostly focuses on refining the unconditional term to improve SDS.

The unconditional term, known for its propensity to introduce over-smoothing artifacts due to mode-seeking characteristics, can be isolated from Eq. (9) as follows:

$$\nabla_\theta \mathcal{L}_{SDS}^{uncond}(\theta) = \mathbb{E}_{t,\epsilon,c} [\omega(t) (\epsilon_\phi(\mathbf{x}_t, t, y) - \epsilon) \frac{\partial \mathbf{x}}{\partial \theta}]. \quad (11)$$

Given that ϵ represents zero-mean Gaussian noise, the expected value of the product $\mathbb{E}_{t,\epsilon,c} [\omega(t) (-\epsilon)] \frac{\partial \mathbf{x}}{\partial \theta}$ is zero. Therefore, the gradient for updating the 3D parameters θ simplifies to $\mathbb{E}_{t,\epsilon,c} [\omega(t) \epsilon_\phi(\mathbf{x}_t, t, y) \frac{\partial \mathbf{x}}{\partial \theta}]$, which steers θ towards the modes of the conditional posterior $p_\phi(\mathbf{x}_t|y)$. However, as SDS involves a multi-step optimization process, the mode achieved is an average of

samples drawn from $p_\phi(\mathbf{x}_t|y)$ for all timestep t , resulting in over-smoothed generative outcomes [WLW*23].

Numerous studies have proposed various strategies to address the challenge of mode-seeking in 3D generation. Our review of recent advancements in refining the standard SDS approach reveals that these efforts generally focus on creating a variational distribution for the rendered images, which shifts the mode-seeking operation to minimizing the KL divergence between two distinct distributions. As illustrated in Table 1, VSD [WLW*23] uses text-conditioned particles (or rendered images when the number of particles equals one) to build a variational distribution of 3D representations. VSD employs a LoRA [HysW*22] model to swiftly optimize the score of rendered images, termed as $\epsilon_{\text{LoRA}}(\mathbf{x}_t, t, y)$. DreamFlow [LSS24] follows VSD with a similar design, guided by theories of Schrodinger Bridge [LVH*23]. ASD [WZSZ23] enhances the optimization methods of VSD within the framework of GAN [GPAM*14], while LODS [YCC*23] diversifies the modeling methods through learnable text embeddings denoted as y_ψ . LMC-SDS [AKS24] pre-trains a neural network to learn the score manifold corrective transitioning rendered images to generated images. The aforementioned studies collectively endeavor to determine the variational distribution of rendered images directly. Despite employing parameter-efficient modeling techniques, i.e., LoRA, the optimization of variational distribution requires additional computation of the UNet Jacobian for Stable Diffusion, which is time-consuming and prone to instability. For instance, given a text prompt, VSD, ASD, and LODs require approximately 8 hours, 5 hours, and 2 hours, respectively to complete the 3D generation. In contrast, DreamFusion only necessitates 1.5 hours since it skips the additional computations on the diffusion model.

Another line of research uses the original Stable Diffusion to approximate the rendered image distribution. CSD [YGL*23] and NFSD [KPCOL24] obtain an empirical solution by using negative prompt conditioned posterior of Stable Diffusion to represent the rendered image distribution. To accommodate the dynamic characteristics of generation, they use iteration steps related weights λ_s and timesteps related weights λ_t separately. ISM [LYL*23] uses DDIM inversion [SME21] to get the score of rendered images. SSD [TWWZ23] applies a closed-form solution $r(\mathbf{x}_t, \epsilon, t, y)$ to project 3D representations to the generated image domain of diffusion models. In Consistent3D [WZY*24], the score of Stable Diffusion in smaller timestep t_2 is treated as the rendered image distribution score. Although this line of research approximates rendered image distribution in a training-free way, the final results may not always be satisfying. Since rendered images during the optimization process are commonly changeable and unnatural, being out-of-domain for the generated image distribution modeled by diffusion models, taking a precise negative prompt or applying a closed-form modeling strategy is unable to model the rendered image generation correctly. Worse still, an additional inference at each optimization iteration is introduced due to negative prompts (e.g., CSD [YGL*23] and NFSD [KPCOL24]).

4.2. Variational Distribution Mapping

During the iterative optimization of SDS, the inferior optimization of 3D object parameters often compromises the quality of rendered

Table 1: Summarize and categorize advancements in SDS. Recent studies primarily concentrate on enhancing SDS through unconditional term refinement. Developing a more adaptable and efficient variational distribution for rendered images improves generation quality.

Method	Unconditional Term	Core Mechanism
SDS [PJBM23]	$\epsilon_\phi(\mathbf{x}_t, t, y) - \epsilon$	Distillation baseline
VSD [WLW*23]	$\epsilon_\phi(\mathbf{x}_t, t, y) - \epsilon_{\text{lorra}}(\mathbf{x}_t, t, y)$	Construct the variational distribution directly with extra models
DreamFlow [LSS24]	$\epsilon_\phi(\mathbf{x}_t, t, y) - \epsilon_{\text{lorra}}(\mathbf{x}_t, t, y)$	
ASD [WZSZ23]	$\epsilon_\phi(\mathbf{x}_t, t, y) - \epsilon_{\text{lorra}}(\mathbf{x}_t, t, y)$	
LODS [YCC*23]	$\epsilon_\phi(\mathbf{x}_t, t, y) - \epsilon_{\text{lorra}}(\mathbf{x}_t, t, y)$ OR $\epsilon_\phi(\mathbf{x}_t, t, y) - \epsilon_\phi(\mathbf{x}_t, t, y_\psi)$	
LMC-SDS [AKS24]	$\epsilon_\phi(\mathbf{x}_t, t, y) - b_\psi(\mathbf{x}_t, t)$	
CSD [YGL*23]	$\epsilon_\phi(\mathbf{x}_t, t, y) - \lambda_s \epsilon_\phi(\mathbf{x}_t, t, y_{\text{neg}})$	Approximate the variational distribution from original Stable Diffusion
NFSD [KPCOL24]	$\epsilon_\phi(\mathbf{x}_t, t, y) - \lambda_t \epsilon_\phi(\mathbf{x}_t, t, y_{\text{neg}})$	
ISM [LYL*23]	$\epsilon_\phi(\mathbf{x}_t, t, y) - \epsilon_\phi(\mathbf{x}_t, s)$	
SSD [TWWZ23]	$\lambda_t (\epsilon_\phi(\mathbf{x}_t, t, y) - r(\mathbf{x}_t, \epsilon, t, y) \cdot \epsilon)$	
Consistent3D [WZY*24]	$\epsilon_\phi(\mathbf{x}_{t_1}, t_1, y) - \epsilon_\phi(\mathbf{x}_{t_2}, t_2, y)$	

images, leading to low-quality (LQ) renderings. Diffusion models face challenges in directly representing low-quality (LQ) images due to limited training in such cases. However, considering the potent capabilities of diffusion models in generating high-quality (HQ) images, it's reasonable to assume they can approximate the HQ counterparts of rendered LQ images by treating the latter as degraded versions of the former. Specifically, given $\hat{\mathbf{x}}_0 \sim p(x)$ as a sample of diffusion output, the rendered image $\mathbf{x}_0 = g(\theta, c)$ can be represented by a degradation result:

$$\mathbf{x}_0 = \mathcal{M}(\hat{\mathbf{x}}_0) + n, \quad (12)$$

where \mathcal{M} is the degradation operator and n is the observation noise. Taking diffusion model outputs as real images, the process in Eq. (12) is a kind of typical real image degradation process [CKM*22].

However, SDS-based 3D generation is a multi-step optimization process with different timestep t , a singular fixed degradation operator cannot represent all the situations. Therefore, as shown in Figure 2, we apply a neural network \mathcal{M}_ψ to model this complex degradation process by learning network weights ψ . According to the experimental results, we omit observation noise n and use \mathcal{M}_ψ to represent the non-linear degradation operator. The learnable degradation process is further formed as:

$$\mathbf{x}_0 = \mathcal{M}_\psi(\hat{\mathbf{x}}_0), \quad (13)$$

where $\hat{\mathbf{x}}_0$ is a sample of the diffusion model generation results, with the posterior $p_\phi(\mathbf{x}_0|y)$ given the text prompt y . The degraded image \mathbf{x}_0 belongs to a learnable variational distribution $q_\psi(\mathbf{x}_0|\hat{\mathbf{x}}_0)$. Our goal is to minimize the KL divergence of rendered images and degraded image distribution, with the formulation as:

$$\min_{\psi} D_{KL}(q^\theta(\mathbf{x}_0) || q_\psi(\mathbf{x}_0|\hat{\mathbf{x}}_0)). \quad (14)$$

Following ProlificDreamer [WLW*23], Eq. (14) can be transferred into a series of optimization problems with different diffused distributions indexed by timestep t . For an arbitrary t , ψ will be optimized from:

$$\min_{\psi} D_{KL}(q^\theta(\mathbf{x}_t) || q_\psi(\mathbf{x}_t|\hat{\mathbf{x}}_t)), \quad (15)$$

where $\mathbf{x}_t = \sqrt{\bar{\alpha}}\mathbf{x}_0 + \sqrt{1 - \bar{\alpha}}\epsilon$ and $\hat{\mathbf{x}}_t = \sqrt{\bar{\alpha}}\mathbf{x}_0 + \sqrt{1 - \bar{\alpha}}\epsilon_\phi(\mathbf{x}_t, t, y)$. Similar to Eq. (7) to Eq. (8), the gradient loss $\nabla_{\psi} \mathcal{L}_{\text{op}}$ to optimize

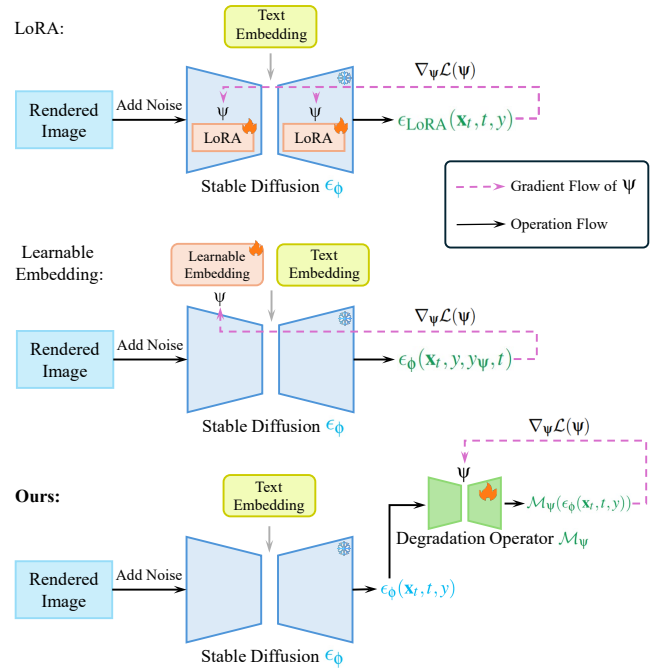


Figure 3: Advantage of VDM. Other solutions modeling the variational distribution of rendered images require extra time to calculate the complex UNet Jacobian matrix in diffusion models. For instance, methods applying LoRA [WLW*23, LSS24, WZSZ23, YCC*23] and Learnable Embedding [YCC*23], when optimizing the variational distribution, the gradient backward must pass through the Stable Diffusion UNet, leading to extra computing time. Our VDM overcomes this problem, taking less time to optimize.

the degradation operator \mathcal{M}_ψ is:

$$\nabla_{\psi} \mathcal{L}_{\text{op}}(\psi) := \nabla_{\psi} \mathbb{E}_{t, \epsilon, c} [||\mathcal{M}_\psi(\hat{\mathbf{x}}_t) - \mathbf{x}_t||_2^2]. \quad (16)$$

Since $\bar{\alpha}$ is a constant pre-defined in diffusion models, for easy calculation, Eq. (16) is equivalent to noise correction [HJA20]:

$$\nabla_{\psi} \mathcal{L}_{\text{op}}(\psi) = \nabla_{\psi} \mathbb{E}_{t, \epsilon, c} [||\mathcal{M}_\psi(\epsilon_\phi(\mathbf{x}_t, t, y)) - \epsilon||_2^2]. \quad (17)$$

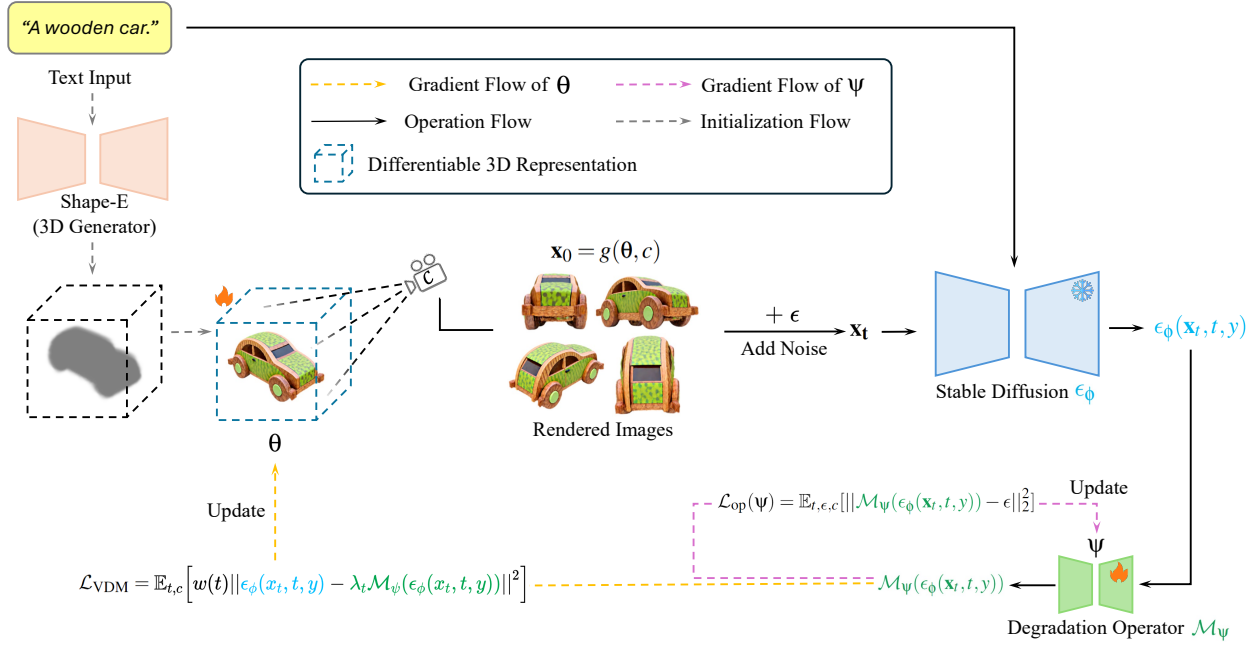


Figure 4: Framework overview. In our text-to-3D generation, we start with the shape initialization (i.e., Shape-E [GYQ*18]) of the 3D representations θ based on the text input y . By incorporating pre-trained Stable Diffusion, we disturb rendered images of random views $\mathbf{x} = g(\theta, c)$ to noisy latents \mathbf{x}_t . After learning the image degradation Ψ , we update θ with the VDM-based loss \mathcal{L}_{VDM} . It is worth noting that the gradient flows bypass the frozen UNet Jacobian terms of Stable Diffusion, significantly expediting the optimization process.

Through optimizing the degradation operator, we learn a variational distribution mapping from the distribution of diffusion models prediction to the rendered image distribution. Compared to other variational distribution modeling methods, a key advantage of VDM is that the optimization of \mathcal{M}_Ψ does not require complex Jacobian matrix calculations in the UNet of the diffusion model, as illustrated in Figure 3.

4.3. Distribution Coefficient Annealing

We further investigate into $\epsilon_\phi(\mathbf{x}_t, t, y)$ with its corresponding score function $\nabla_{\mathbf{x}_t} \log p(\mathbf{x}_t|y)$, analyzing its properties and finding different features in different timesteps. Specifically, when the timestep becomes large, $t \rightarrow T$ and $\bar{\alpha}_t \rightarrow 0$. The added noise $\sqrt{1 - \bar{\alpha}_t}\epsilon$ tends to have a relatively large value and high variance. Based on this, if we seek a special mode from the posterior $p_\phi(\mathbf{x}_t|y)$ to guide the optimization of 3D objects at large timesteps, the guidance will also have high variance and lead to over-smoothing results (refer to Figure 11). When the timestep t is small, however, the mode-seeking behavior is precisely what we want to retrieve since $p_\phi(\mathbf{x}_t|y) \approx p_\phi(\mathbf{x}|y)$.

Additionally, we find that our design of VDM may not work perfectly at small timesteps, as the modeling of the degradation process builds on the assumption that at least ϵ and ϵ_ϕ are associated. Nonetheless, the linear correlation between ϵ and $\epsilon_\phi(\mathbf{x}_t, t, y)$ as defined in [Puc22] is anticipated to diminish as t decreases (shown in Figure 11 and proved in Sec. 7.1), which means $\epsilon_\phi(\mathbf{x}_t, t, y)$ becomes independent of ϵ when t is small [TWWZ23]. Consequently,

VDM may not flawlessly work alone in small timesteps, where mode-seeking is beneficial, as well as $\epsilon_\phi(\mathbf{x}_t, t, y)$ and ϵ are unrelated. To address this, we propose the distribution coefficient annealing (DCA) strategy for better 3D generation, which adds a time-dependent coefficient λ_t to the rendered image distribution. λ_t is calculated by:

$$\lambda_t = \begin{cases} 1, & t > 300 \\ 1 - \bar{\alpha}_t, & t \leq 300, \end{cases} \quad (18)$$

and the final gradient of VDM loss over 3D parameters θ is:

$$\nabla_{\theta} \mathcal{L}_{\text{VDM}} = \mathbb{E}_{t,c} [\omega(t) (\epsilon_\phi(\mathbf{x}_t, t, y) - \lambda_t \mathcal{M}_\Psi(\epsilon_\phi(\mathbf{x}_t, t, y))) \frac{\partial \mathbf{x}_t}{\partial \theta}]. \quad (19)$$

The Jacobian term $\frac{\partial \epsilon_\phi(\mathbf{x}_t, t, y) - \lambda_t \mathcal{M}_\Psi(\epsilon_\phi(\mathbf{x}_t, t, y))}{\partial \mathbf{x}_t}$ is also ignored following the conclusion of SDS [PJBM23].

4.4. Generation Framework

Following recent text-to-3D generation methods [PJBM23, WLW*23, CCJJ23], our optimized-based framework leverages 3D Gaussian Splatting (3DGS), which is highly efficient in rendering to high-fidelity 3D creations. As Liang et al. [LYL*23] have demonstrated, point cloud initialization is critical for geometry quality. We adopt Shape-E [JN23] to generate the coarse initialization with shape prior (Figure 4). Algorithm 1 shows the 3D generation process of DreamMapping.

Table 2: Quantitative comparison with text-to-3D methods on generation consistency. The CLIP score [RKH*21] measures the semantic similarity between text prompts and randomly rendered views. Generation time measures averaged time cost per text prompt. ViT-L/14 and ViT-bigG-14 represent two different backbones used to calculate the CLIP score.

Method	ViT-L/14 (\uparrow)	ViT-bigG-14 (\uparrow)	Generation Time(\downarrow)
Shap-E [JN23]	20.51	32.21	6 seconds
DreamFusion [PJB23]	23.60	37.46	1.5 hours
DreamGaussian [TRZ*23]	20.85	30.51	5 minutes
GaussianDreamer [YFW*24]	27.23	41.88	15 minutes
ProlificDreamer [WLW*23]	27.39	42.98	10 hours
Ours	30.16	42.10	15 minutes

Algorithm 1: The generation pipeline of DreamMapping

Input: Large text-to-image diffusion model ϵ_ϕ , 3D object initialized by Shap-E with parameters θ , learnable operator \mathcal{M}_ψ , text prompt y

```

1 while  $\theta$  not converged do
2   Randomly sample a camera pose  $c$ ;
3   Render the 3D object at pose  $c$  to get a 2D image
    $\mathbf{x}_0 = g(\theta, c)$ ;
4   Sample  $\epsilon \sim \mathcal{N}(0, I), t \sim \mathcal{U}(0, 1000)$ ;
5    $\mathbf{x}_t = \sqrt{\bar{\alpha}_t} \mathbf{x} + \sqrt{1 - \bar{\alpha}_t} \epsilon$ ;
6   if  $t < 300$  then
7      $\lambda_t = 1 - \bar{\alpha}_t$ ;
8   else
9      $\lambda_t = 1$ ;
10   $\mathcal{L}_{op} = \mathbb{E}_{t, \epsilon, c} [ \|\mathcal{M}_\psi(\epsilon_\phi(\mathbf{x}_t, t, y)) - \epsilon\|_2^2 ]$ ;
11   $\mathcal{L}_{VDM} = \mathbb{E}_{t, \epsilon, c} [ \|\omega(t) | \epsilon_\phi(\mathbf{x}_t, t, y) - \lambda_t \mathcal{M}_\psi(\epsilon_\phi(\mathbf{x}_t, t, y)) \|_2^2 ]$ ;
12  Update  $\psi$  with  $\nabla_\psi \mathcal{L}_{op}$ ;
13  Update  $\theta$  with  $\nabla_\theta \mathcal{L}_{VDM}$ ;

```

5. Experiments

The diverse 3D models generated through our framework are demonstrated in Figures 1 and 13. Our framework can produce 3D assets that align closely with textual semantics, presenting fine appearances and detailed features. It effectively handles creative long-text descriptions, such as ‘‘A Spanish galleon sailing on the open sea’’ (Figure 1), while mitigating excess smoothness and color saturation issues, for instance, in fur textures or layered burritos. This section first discusses the choice of 3D representations and outlines the implementation details of our generation framework, followed by experiments and a user study to compare our outcomes with those produced by state-of-the-art (SoTA) methods. An ablation study is then conducted to assess the effectiveness of key design choices in our approach.

5.1. Choice of 3D Representation

In this study, we used 3DGS as the primary 3D representation and also showed the efficacy of our proposed method on NeRF (Figure 9). Compared to NeRF, 3DGS offers several advantages:

- Efficiency. 3DGS outperforms NeRF in rendering and optimiza-

tion efficiency (i.e., less generation time and lower GPU usage). ProlificDreamer uses NeRF for high-quality 3D generation but is time-consuming (10 hours), as shown in Table 2.

- Explicitly. 3DGS is an explicit 3D representation and can be adapted to traditional graphics pipelines. Recent works have successfully applied 3DGS in Unity [JYX*24, SWL*24].
- Versatility. Several concurrent works (e.g., 2DGS [HYC*24] and GoF [YSG24]) have been put forward to improve the geometry structure of 3DGS. These studies demonstrate optimization and rendering efficiency comparable to the original 3DGS. However, improvements to NeRF such as Mip-NeRF360 [BMV*22] present an unacceptable long training time.

5.2. Implementation Details

We employed the codebase from LucidDreamer [LYL*23] and replaced the ISM loss with our proposed VDM and DCA. Stable-Diffusion-2-1-Base (SD 2.1 Base) [Stab] was utilized as the base diffusion model ϵ_ϕ . For the geometry initialization, we used Shap-E [JN23] as the prior point cloud generator and upsampling the number of initialization points to nearly 50000. The batch size is set to 4, and the optimization iterations for each 3D object is 5000. For the learnable operator \mathcal{M}_ψ , we selected U-Lite [DNTP23], a kind of UNet [RFB15] with only $1M$ parameters in the learnable neural network. The learning rate of \mathcal{M}_ψ is 0.01 to efficiently model the degradation process.

5.3. Quantitative Results

We performed comprehensive experiments to assess the semantic coherence (CLIP-score) and visual quality (3D-FID) of the generated 3D content. The quantitative results presented in Table 2 and Table 3 indicate that our method outperforms state-of-the-art 3DGS-based methods in terms of rendering appearance and multi-view semantic consistency. Although ProlificDreamer attains the highest CLIP score on ViT-bigG-14 [RKH*21], its generation time is considerably longer than DreamFusion, which also employs the NeRF representation. This is attributed to the time-consuming process of constructing a variational distribution in ProlificDreamer. In contrast, our approach efficiently constructs a variational distribution with a generation time comparable to GaussianDreamer, which does not build such a distribution. To further demonstrate the efficiency and quality of our methods, we implemented NeRF with VDM and DCA (seen in Figure 9), achieving a generation time of approximately 1.9 hours per text prompt on a single A100 GPU.

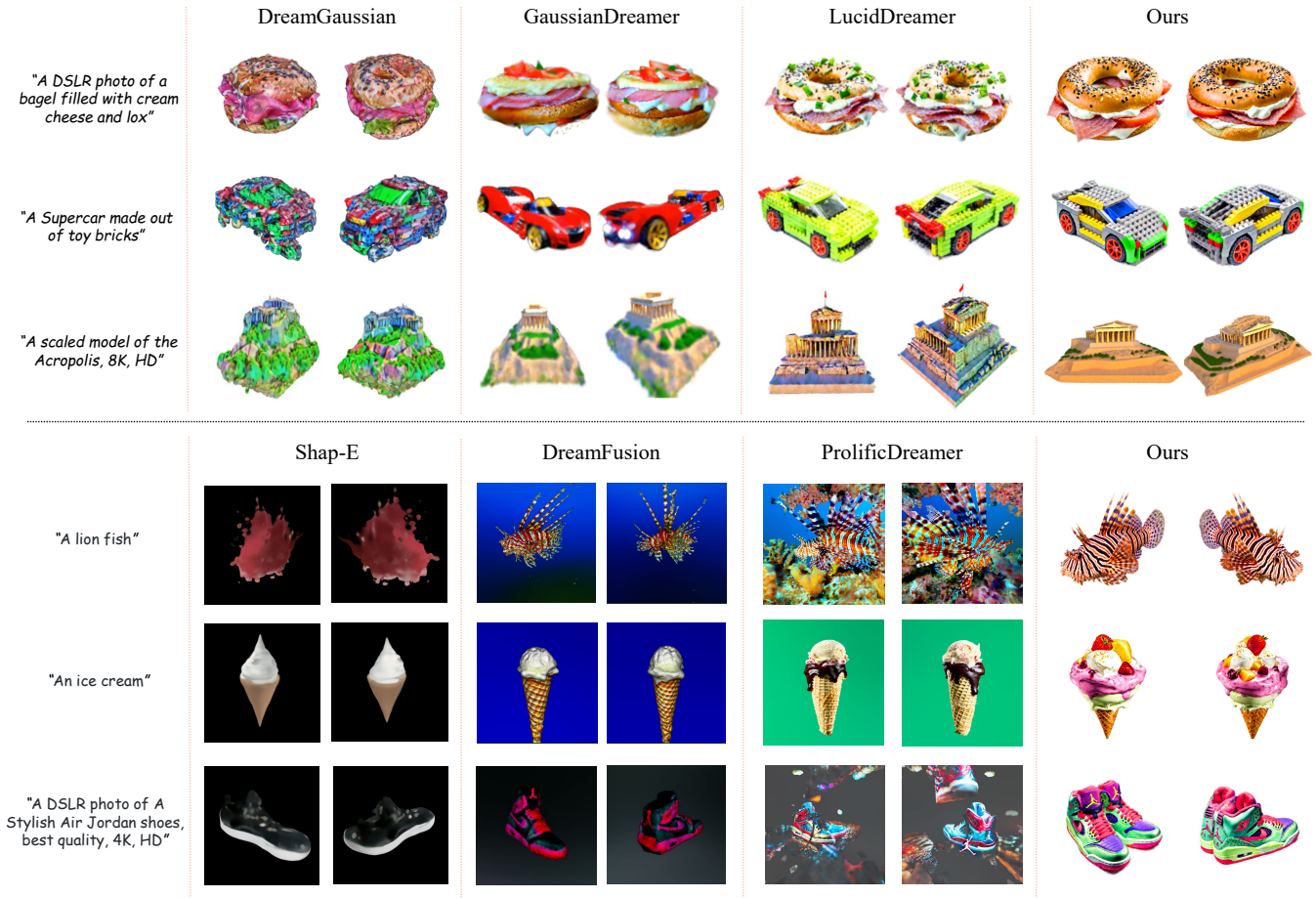


Figure 5: Qualitative comparisons with recent popular methods in text-to-3D generation based on 3DGS and NeRF. We present rendered images of two views for each method. Experimental results demonstrate that our method generates 3D content closely aligned with textual prompts, exhibiting high fidelity and intricate details. Please zoom in for details. Additional comparisons can be found in Figure 12.

We believe our quantitative evaluation will inform future research utilizing 3DGS-based generation.

Table 3: Quantitative comparison with text-to-3D methods on generation appearance. The 3D-FID [WLW*23] is evaluated between rendered images of random views and reference images sampled by 50-step DPM-Solver++ [LZB*23]. ↓ indicates lower is better.

Method	3D-FID ↓ (25 Prompts)
SDS [PJB23]	191.82
ProlificDreamer [WLW*23]	159.84
DreamGaussian [TRZ*23]	265.88
GaussianDreamer [YFW*24]	156.71
LucidDreamer [LYL*23]	142.63
Ours	139.03

5.4. Qualitative Results

We compared our model with current SoTA baselines using 3DGS representation (i.e., DreamGaussian [TRZ*23], Gaussian-

Table 4: User preferences. Small values indicate high rankings. Our results achieved the highest ranking.

	Semantic Alignment	Generation Quality
DreamGaussian [TRZ*23]	4.94	4.83
ProlificDreamer [WLW*23]	<u>2.50</u>	<u>2.34</u>
GaussianDreamer [YFW*24]	3.72	3.80
LucidDreamer [LYL*23]	2.78	2.54
Ours	1.05	1.49

Dreamer [YFW*24], LucidDreamer [LYL*23]). SD 2.1 Base was used for distillation, and all generation experiments were conducted on Nvidia A100 for fair comparison. As shown in Figure 5, we can see that DreamGaussian suffers from low quality with blurry appearance and incomplete shape. Results of GaussianDreamer and LucidDreamer show good semantic consistency and realistic colors. However, they still generate vague textures on parts of generated models. For example, the tail light part in the case of “A supercar made out of toy bricks” is blurry, and fur details are missing in

GaussianDreamer. Instead, our approach efficiently predicts an accurate variational distribution of rendered images, yielding diverse semantically meaningful 3D assets with clear geometry structure and intricate appearance details. Lastly, it is important to highlight that LucidDreamer’s generation time is typically longer than our approach due to its use of the DDIM inversion method [SME21], which requires substantially more computational resources, such as loss computations. Please refer to Figure 13 more visual results.

5.5. User Study

To present real-world user preferences, we conducted a user study to provide a comprehensive evaluation. Specifically, we select 28 text prompts from ViT-L/14 [RKH*21] to render multiple views using different text-to-3D frameworks. 36 Users, of whom 26 are graduate students majoring in computer graphics and vision and 10 are company employees specializing in AI content generation, were invited to rank them based on the rendering fidelity and the degree of semantic alignment with given text descriptions. As shown in Table 4, our framework achieves the highest average ranking, indicating that our approach significantly outperforms existing methods in text-to-3D tasks with respect to human preferences.

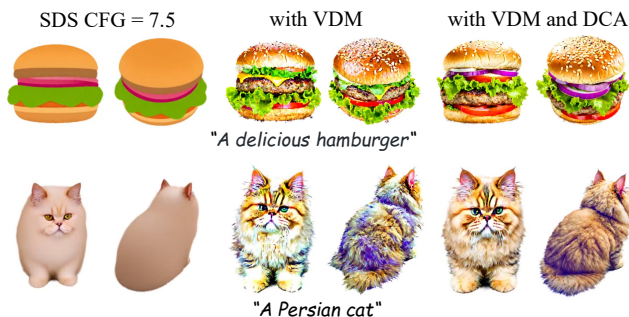


Figure 6: Ablation study on EDM and DCA. Compared to SDS, EDM significantly adds appearance details to 3D models, and DCA further controls color saturation.

5.6. Ablation Study

Effect of VDM and DCA. We examine the impact of our proposed VDM and DCA. As illustrated in Figure 6, when the CFG scale is set to 7.5, the original SDS produces overly smooth 3D appearance. Incorporating VDM enhances the visual details of generated 3D assets but leads to slight color saturation and persistent noise issues. By integrating both VDM and DCA, our framework is capable of generating highly detailed and realistic 3D models.

Discussion on the degradation process. In Sec. 4.2, we model the degradation relationship between diffusion model-generated images and rendered images using a learnable nonlinear degradation operator without observation noise, which is the most important design of VDM. We evaluated three different degradation settings to validate our selection. Figure 7 reveals that nonlinear operators outperform linear ones, which are implemented as a learnable tensor matching the dimensions of $\epsilon_\phi(\mathbf{x}_t, t, y)$. 3D results from linear

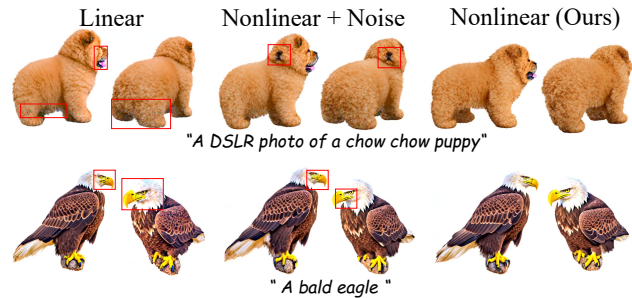


Figure 7: Ablation study on designs of the image degradation process. We show the effects of modeling this degradation with the linear learnable operator, nonlinear learnable operator with noise, and our choice, a noise-free nonlinear learnable operator (M_ψ).

operators exhibit more noise due to limited modeling capacity. Furthermore, the inclusion of learnable observation noise, denoted by a tensor equivalent in size to the predicted noise, fails to enhance 3D generation and may introduce artifacts in some instances.

Choice of timestep in DCA. In the execution of DCA, as outlined in Eq. (18), we select a specific timestep $t = 300$ as the cut-off point to tune the coefficient λ_t of rendered image distribution. As illustrated in Figure 8, we conduct experiments to substantiate the efficacy of our selection. When the timestep is set to 100, the generated 3D results are analogous to those without DCA, exhibiting color-saturation problems and some noise artifacts. Conversely, increasing the cut-off timestep to 500 leads to excess smoothness issues, and the rendering is similar to the result through the utilization of SDS with a CFG scaling factor of 7.5. Consequently, opting for a time step $t = 300$ enables DreamMapping to generate high-quality 3D objects with realistic color and fewer artifacts.

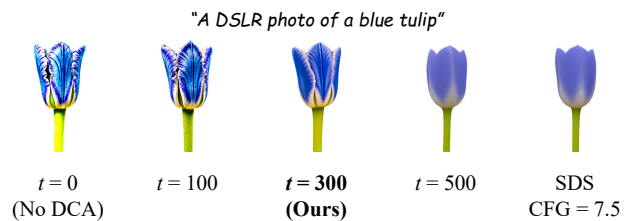


Figure 8: Ablation study on different timestep choice of DCA.

Generalizability of DreamMapping. Although we integrate VDM and DCA into the 3DGS-based text-to-3D framework, their generative potential can be extended beyond this context. Our improvements on SDS can be applied to other 3D representations as well, e.g., NeRF [MST*20]. As depicted in Figure 9, we follow the hyperparameter configurations employed by ProlificDreamer [WLW*23] in NeRF comparison experiments. Remarkably, our proposed method can deliver intricate details even under a CFG setting of 7.5. A particularly noteworthy aspect is the generation time afforded by our approach when integrated with NeRF, averaging approximately 1.9 hours, significantly shorter than ProficiDreamer. This efficiency gain primarily stems

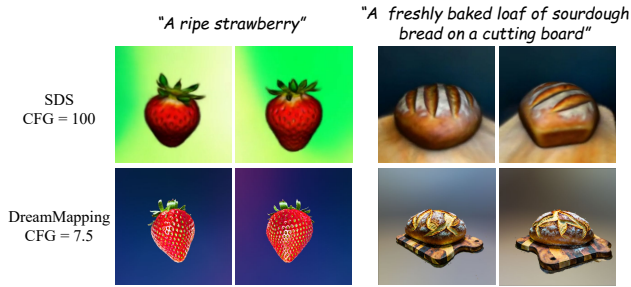


Figure 9: Generalizability of DreamMapping on NeRF.

from the construction of a variational distribution within our optimization framework, which bypasses the gradient computation for the Unet Jacobian term in diffusion models. Additionally, VDM and DCA methods can be seamlessly integrated into text-to-2D generation, exhibiting style-matching results with rich details and optimization efficiency, as shown in Figures 10 and 14.

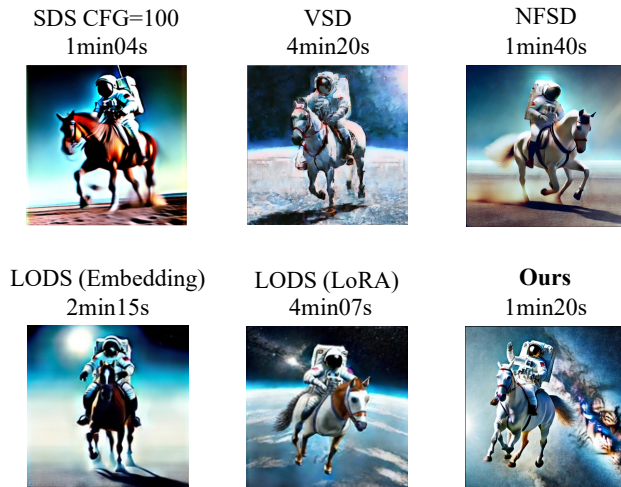


Figure 10: Qualitative comparisons for text-to-2D task. Our method displays clear details and mitigates color saturation issues. The experiment of generation time comparison was conducted on a single NVIDIA 4090 GPU.

6. Conclusion

In this work, we have presented a comprehensive analysis and review of SDS-based methods. We further concluded their defects in dealing with the variational distribution. Based on the analysis, we have proposed Variational Distribution Mapping (VDM) with Distribution Coefficient Annealing (DCA), a novel approach for constructing an efficient variational distribution through a learnable neural network without refining the diffusion model.

Building upon this, we have developed DreamMapping, a text-to-3D framework that integrates VDM and DCA with 3D Gaussian Splatting. Through extensive experiments and evaluations, we validate the effectiveness of our approach. Notably, our approach’s

compatibility can be extended to other 3D representations, e.g., NeRF and text-to-2D generation.

While DreamMapping can produce diverse high-fidelity 3D assets, it still has several limitations for further improvements. First, the generation quality of our framework relies heavily on geometry initialization. Second, the timestep choice of DCA could become a learnable factor, adapting to the diffusion model’s dynamic characteristics. Besides, exploring the training of an independent image distribution model before the generation task may offer opportunities to expedite generation time in future research.

Acknowledgments

We thank Dr. Ailing Zeng for the insightful discussions and all the participants for evaluating our results. This project is partially supported by the CCF-Tencent Rhino-Bird Open Research Fund RAGR20230120 and the Open Project Program of the State Key Laboratory of CAD&CG (Grant No. A2427), Zhejiang University.

References

- [AKS24] ALLDIECK T., KOLOTOUROS N., SMINCHISDESCU C.: Score Distillation Sampling with Learned Manifold Corrective. *arXiv preprint 2401.05293* (2024). [2](#), [3](#), [4](#), [5](#)
- [ASZ*23] ARMANDPOUR M., SADEGHIAN A., ZHENG H., SADEGHIAN A., ZHOU M.: Re-imagine the Negative Prompt Algorithm: Transform 2D Diffusion into 3D, alleviate Janus problem and Beyond. *arXiv preprint 2304.04968* (2023). [3](#)
- [BMV*22] BARRON J. T., MILDENHALL B., VERBIN D., SRINIVASAN P. P., HEDMAN P.: Mip-NeRF 360: Unbounded Anti-aliased Neural Radiance Fields. In *Proceedings of the IEEE/CVF Conference on Computer Vision and Pattern Recognition* (2022), pp. 5470–5479. [7](#)
- [CCH*23] CAO Y., CAO Y.-P., HAN K., SHAN Y., WONG K.-Y. K.: DreamAvatar: Text-and-shape Guided 3D Human Avatar Generation via Diffusion Models. *arXiv preprint 2304.00916* (2023). [2](#)
- [CCJJ23] CHEN R., CHEN Y., JIAO N., JIA K.: Fantasia3D: Disentangling Geometry and Appearance for High-quality Text-to-3D Content Creation. In *Proceedings of the IEEE/CVF International Conference on Computer Vision* (October 2023), pp. 22246–22256. [2](#), [3](#), [6](#)
- [CKM*22] CHUNG H., KIM J., MCCANN M. T., KLASKY M. L., YE J. C.: Diffusion Posterior Sampling for General Noisy Inverse Problems. In *The Eleventh International Conference on Learning Representations* (2022). [5](#)
- [CT14] CHENG K.-H., TSAI C.-C.: Children and Parents’ Reading of An Augmented Reality Picture Book: Analyses of Behavioral Patterns and Cognitive Attainment. *Computers & Education* 72 (2014), 302–312. [2](#)
- [DN24] DHARIWAL P., NICHOL A.: Diffusion Models Beat GANs on Image Synthesis. In *Proceedings of the 35th International Conference on Neural Information Processing Systems* (Red Hook, NY, USA, 2024), Curran Associates Inc. [2](#)
- [DNTP23] DINH B.-D., NGUYEN T.-T., TRAN T.-T., PHAM V.-T.: 1M Parameters Are Enough? A Lightweight CNN-based Model for Medical Image Segmentation. In *2023 Asia Pacific Signal and Information Processing Association Annual Summit and Conference (APSIPA ASC)* (2023), pp. 1279–1284. [7](#)
- [GAG*23] GAO W., AIGERMAN N., GROUEIX T., KIM V., HANOCKA R.: TextDeformer: Geometry Manipulation Using Text Guidance. In *ACM SIGGRAPH 2023 Conference Proceedings* (New York, NY, USA, 2023), SIGGRAPH ’23, Association for Computing Machinery. [3](#)

- [Ger12] GERSHENFELD N.: How to Make Almost Anything: The Digital Fabrication Revolution. *Foreign Aff.* 91 (2012), 43. 2
- [GPAM*14] GOODFELLOW I. J., POUGET-ABADIE J., MIRZA M., XU B., WARDE-FARLEY D., OZAIR S., COURVILLE A., BENGIO Y.: Generative Adversarial Nets. In *Proceedings of the 27th International Conference on Neural Information Processing Systems - Volume 2* (Cambridge, MA, USA, 2014), MIT Press, p. 2672–2680. 4
- [GYQ*18] GAO L., YANG J., QIAO Y.-L., LAI Y.-K., ROSIN P. L., XU W., XIA S.: Automatic Unpaired Shape Deformation Transfer. *ACM Trans. Graph.* 37, 6 (Dec 2018). 6
- [HAK23] HONG S., AHN D., KIM S.: Debiasing Scores and Prompts of 2D Diffusion for View-consistent Text-to-3D Generation. In *Neural Information Processing Systems* (2023). 3
- [HJA20] HO J., JAIN A., ABBEEL P.: Denoising Diffusion Probabilistic Models. In *Proceedings of the 34th International Conference on Neural Information Processing Systems* (Red Hook, NY, USA, 2020), Curran Associates Inc. 2, 3, 5
- [HS21] HO J., SALIMANS T.: Classifier-Free Diffusion Guidance. In *NeurIPS 2021 Workshop on Deep Generative Models and Downstream Applications* (2021). 2, 3
- [HWW*21] HEALEY J., WANG D., WINGTON C., SUN T., PENG H.: A Mixed-Reality System to Promote Child Engagement in Remote Intergenerational Storytelling. In *2021 IEEE International Symposium on Mixed and Augmented Reality Adjunct (ISMAR-Adjunct)* (2021), pp. 274–279. 2
- [HYC*24] HUANG B., YU Z., CHEN A., GEIGER A., GAO S.: 2D Gaussian Splatting for Geometrically Accurate Radiance Fields. In *ACM SIGGRAPH 2024 Conference Papers* (2024), pp. 1–11. 7
- [HysW*22] HU E. J., YELONG SHEN, WALLIS P., ALLEN-ZHU Z., LI Y., WANG S., WANG L., CHEN W.: LoRA: Low-rank adaptation of large language models. In *International Conference on Learning Representations* (2022). 4
- [JMB*22] JAIN A., MILDENHALL B., BARRON J. T., ABBEEL P., POOLE B.: Zero-Shot Text-Guided Object Generation With Dream Fields. In *Proceedings of the IEEE/CVF Conference on Computer Vision and Pattern Recognition* (June 2022), pp. 867–876. 2
- [JN23] JUN H., NICHOL A.: Shap-E: Generating Conditional 3D Implicit Functions. *arXiv preprint 2305.02463* (2023). 2, 6, 7
- [JYX*24] JIANG Y., YU C., XIE T., LI X., FENG Y., WANG H., LI M., LAU H., GAO F., YANG Y., ET AL.: VR-GS: a Physical Dynamics-Aware Interactive Gaussian Splatting System in Virtual Reality. In *ACM SIGGRAPH 2024 Conference Papers* (2024), pp. 1–1. 7
- [KKLD23] KERBL B., KOPANAS G., LEIMKUEHLER T., DRETTAKIS G.: 3d gaussian splatting for real-time radiance field rendering. *ACM Trans. Graph.* 42, 4 (jul 2023). 2, 3
- [KPCOL24] KATZIR O., PATASHNIK O., COHEN-OR D., LISCHINSKI D.: Noise-free Score Distillation. In *The Twelfth International Conference on Learning Representations* (2024). 2, 3, 4, 5
- [LGT*23] LIN C.-H., GAO J., TANG L., TAKIKAWA T., ZENG X., HUANG X., KREIS K., FIDLER S., LIU M.-Y., LIN T.-Y.: Magic3D: High-Resolution Text-to-3D Content Creation. In *Proceedings of the IEEE/CVF Conference on Computer Vision and Pattern Recognition* (2023), pp. 300–309. 2, 3
- [LSS24] LEE K., SOHN K., SHIN J.: DreamFlow: High-Quality Text-to-3D Generation by Approximating Probability Flow. *arXiv preprint 2403.14966* (2024). 2, 4, 5
- [LVH*23] LIU G.-H., VAHDAT A., HUANG D.-A., THEODOROU E. A., NIE W., ANANDKUMAR A.: I²sb: Image-to-image schrödinger bridge. In *International Conference on Machine Learning* (2023). 4
- [LWH*23] LIU R., WU R., HOORICK B. V., TOKMAKOV P., ZAKHAROV S., VONDRICK C.: Zero-1-to-3: Zero-shot One Image to 3D Object. *2023 IEEE/CVF International Conference on Computer Vision* (2023), 9264–9275. 3
- [LWW*23] LIU H., WANG X., WAN Z., SHEN Y., SONG Y., LIAO J., CHEN Q.: HeadArtist: Text-conditioned 3D Head Generation with Self Score Distillation. *arXiv preprint 2312.07539* (2023). 3
- [LYB*24] LIM S., YOON E., BYUN T., KANG T., KIM S., LEE K., CHOI S.: Score-based Generative Modeling through Stochastic Evolution Equations in Hilbert Spaces. In *Proceedings of the 37th International Conference on Neural Information Processing Systems* (Red Hook, NY, USA, 2024), Curran Associates Inc. 3
- [LYL*23] LIANG Y., YANG X., LIN J., LI H., XU X., CHEN Y.: LucidDreamer: Towards High-Fidelity Text-to-3D Generation via Interval Score Matching. *arXiv preprint 2311.11284* (2023). 2, 3, 4, 5, 6, 7, 8
- [LZB*23] LU C., ZHOU Y., BAO F., CHEN J., LI C., ZHU J.: DPM-Solver++: Fast Solver for Guided Sampling of Diffusion Probabilistic Models. *arXiv preprint 2211.01095* (2023). 8
- [MRP*22] METZER G., RICHARDSON E., PATASHNIK O., GIRYES R., COHEN-OR D.: Latent-NeRF for Shape-Guided Generation of 3D Shapes and Textures. In *Proceedings of the IEEE/CVF Conference on Computer Vision and Pattern Recognition* (2022), pp. 12663–12673. 3
- [MST*20] MILDENHALL B., SRINIVASAN P. P., TANCIK M., BARRON J. T., RAMAMOORTHI R., NG R.: NeRF: Representing Scenes as Neural Radiance Fields for View Synthesis. In *European Conference on Computer Vision (ECCV)* (2020), pp. 405–421. 3, 9
- [PBJM23] POOLE B., JAIN A., BARRON J. T., MILDENHALL B.: DreamFusion: Text-to-3D using 2D Diffusion. In *The Eleventh International Conference on Learning Representations* (2023). 2, 3, 4, 5, 6, 7, 8
- [Puc22] PUCETTI G.: Measuring Linear Correlation between Random Vectors. *Information Sciences* 607 (2022), 1328–1347. 6
- [RBL*22] ROMBACH R., BLATTMANN A., LORENZ D., ESSER P., OMMER B.: High-Resolution Image Synthesis with Latent Diffusion Models. *Proceedings of the IEEE/CVF Conference on Computer Vision and Pattern Recognition* (2022), 10674–10685. 2, 3, 4
- [RFB15] RONNEBERGER O., FISCHER P., BROX T.: U-Net: Convolutional Networks for Biomedical Image Segmentation. In *Medical Image Computing and Computer-Assisted Intervention – MICCAI 2015* (Cham, 2015), Navab N., Hornegger J., Wells W. M., Frangi A. F., (Eds.), Springer International Publishing, pp. 234–241. 3, 7
- [RKH*21] RADFORD A., KIM J. W., HALLACY C., RAMESH A., GOH G., AGARWAL S., SASTRY G., ASKELL A., MISHKIN P., CLARK J., KRUEGER G., SUTSKEVER I.: Learning Transferable Visual Models From Natural Language Supervision. In *International Conference on Machine Learning* (2021). 7, 9
- [SCS*22] SAHARIA C., CHAN W., SAXENA S., LI L., WHANG J., DENTON E. L., GHASEMPOUR K., GONTIJO LOPES R., KARAGOL AYAN B., SALIMANS T., HO J., FLEET D. J., NOROUZI M.: Photorealistic Text-to-Image Diffusion Models with Deep Language Understanding. In *Advances in Neural Information Processing Systems* (2022), Koyejo S., Mohamed S., Agarwal A., Belgrave D., Cho K., Oh A., (Eds.), vol. 35, Curran Associates, Inc., pp. 36479–36494. 3
- [SE19] SONG Y., ERMON S.: Generative Modeling by Estimating Gradients of the Data Distribution. In *Advances in Neural Information Processing Systems* (2019), Wallach H., Larochelle H., Beygelzimer A., d'Alché-Buc F., Fox E., Garnett R., (Eds.), vol. 32, Curran Associates, Inc. 3
- [SGY*21] SHEN T., GAO J., YIN K., LIU M.-Y., FIDLER S.: Deep Marching Tetrahedra: a Hybrid Representation for High-resolution 3D Shape Synthesis. *Advances in Neural Information Processing Systems* 34 (2021), 6087–6101. 3
- [SME21] SONG J., MENG C., ERMON S.: Denoising Diffusion Implicit Models. In *International Conference on Learning Representations* (2021). 2, 3, 4, 9
- [Staa] STABILITYAI: Dreamshaper-v7. [EB/OL]. Accessed April 6th, 2024. URL: <https://huggingface.co/stablediffusionapi/dreamshaper-v7>. 15

- [Stab] STABILITYAI: Stable Diffusion 2-1-base. [EB/OL]. Accessed April 4th, 2024. URL: <https://huggingface.co/stabilityai/stable-diffusion-2-1-base>. 7, 15
- [SWL*24] SHAO Z., WANG Z., LI Z., WANG D., LIN X., ZHANG Y., FAN M., WANG Z.: SplattingAvatar: Realistic Real-time Human Avatars with Mesh-embedded Gaussian Splatting. In *Proceedings of the IEEE/CVF Conference on Computer Vision and Pattern Recognition* (2024), pp. 1606–1616. 7
- [SWY*24] SHI Y., WANG P., YE J., MAI L., LI K., YANG X.: MV-Dream: Multi-view Diffusion for 3D Generation. In *The Twelfth International Conference on Learning Representations* (2024). 3
- [TMT*24] TSALICOGLU C., MANHARDT F., TONIONI A., NIEMEYER M., TOMBARI F.: TextMesh: Generation of Realistic 3D Meshes from Text Prompts. In *International Conference on 3D Vision (3DV)* (2024), IEEE, pp. 1554–1563. 3
- [TRZ*23] TANG J., REN J., ZHOU H., LIU Z., ZENG G.: Dream-gaussian: Generative gaussian splatting for efficient 3d content creation. *arXiv preprint 2309.16653* (2023). 3, 7, 8
- [TWWZ23] TANG B., WANG J., WU Z., ZHANG L.: Stable Score Distillation for High-Quality 3D Generation. *arXiv preprint 2312.09305* (2023). 2, 4, 5, 6, 13
- [TWZ*23] TANG J., WANG T., ZHANG B., ZHANG T., YI R., MA L., CHEN D.: Make-It-3D: High-fidelity 3D Creation from A Single Image with Diffusion Prior. In *Proceedings of the IEEE/CVF International Conference on Computer Vision* (October 2023), pp. 22819–22829. 3
- [WDL*23] WANG H., DU X., LI J., YEH R. A., SHAKHAROVICH G.: Score Jacobian Chaining: Lifting Pretrained 2D Diffusion Models for 3D Generation. In *Proceedings of the IEEE/CVF Conference on Computer Vision and Pattern Recognition* (2023), pp. 12619–12629. 2, 3
- [WLW*23] WANG Z., LU C., WANG Y., BAO F., LI C., SU H., ZHU J.: ProlificDreamer: High-Fidelity and Diverse Text-to-3D Generation with Variational Score Distillation. In *Thirty-seventh Conference on Neural Information Processing Systems* (2023). 2, 3, 4, 5, 6, 7, 8, 9
- [WMC*24] WANG D., MENG H., CAI Z., SHAO Z., LIU Q., WANG L., FAN M., SHAN Y., ZHAN X., WANG Z.: HeadEvolver: Text to Head Avatars via Locally Learnable Mesh Deformation. *ArXiv abs/2403.09326* (2024). 3
- [WXF*23] WANG P., XU D., FAN Z., WANG D., MOHAN S., IANDOLA F. N., RANJAN R., LI Y., LIU Q., WANG Z., CHANDRA V.: Taming Mode Collapse in Score Distillation for Text-to-3D Generation. *arXiv preprint 2401.00909* (2023). 3
- [WZSZ23] WEI M., ZHOU J., SUN J., ZHANG X.: Adversarial Score Distillation: When Score Distillation Meets GAN. *arXiv preprint 2312.00739* (2023). 2, 4, 5
- [WZY*24] WU Z., ZHOU P., YI X., YUAN X., ZHANG H.: Consistent3D: Towards Consistent High-Fidelity Text-to-3D Generation with Deterministic Sampling Prior. *arXiv preprint 2401.09050* (2024). 2, 4, 5
- [YCC*23] YANG X., CHEN Y., CHEN C., ZHANG C., XU Y., YANG X., LIU F., LIN G.: Learn to Optimize Denoising Scores for 3D Generation: A Unified and Improved Diffusion Prior on NeRF and 3D Gaussian Splatting. *arXiv preprint 2312.04820* (2023). 2, 4, 5
- [YFW*24] YI T., FANG J., WANG J., WU G., XIE L., ZHANG X., LIU W., TIAN Q., WANG X.: GaussianDreamer: Fast Generation from Text to 3D Gaussians by Bridging 2D and 3D Diffusion Models. In *Proceedings of the IEEE/CVF Conference on Computer Vision and Pattern Recognition* (June 2024), pp. 6796–6807. 3, 7, 8
- [YGL*23] YU X., GUO Y., LI Y., LIANG D., ZHANG S.-H., QI X.: Text-to-3D with Classifier Score Distillation. *arXiv preprint 2310.19415* (2023). 2, 3, 4, 5
- [YSG24] YU Z., SATTTLER T., GEIGER A.: Gaussian Opacity Fields: Efficient and Compact Surface Reconstruction in Unbounded Scenes. *arXiv preprint 2404.10772* (2024). 7
- [ZW12] ZACKARIASSON P., WILSON T. L.: *The Video Game Industry: Formation, Present State, and Future*. Routledge, 2012. 2

7. Appendix

7.1. Analysis for DCA

Recalling our DCA discussion, we made a simplified assumption, using a timestep $t = 300$ as the cut-off point for adjusting λ . Besides the ablation study in Sec. 5.6, here we substantiate this design and statement that the linear correlation between ϵ and $\epsilon_\phi(\mathbf{x}_t, t, y)$ becomes independent at a small timestep t .

As outlined in Eq. (3), the score function $\nabla_{\mathbf{x}_t} \log p(\mathbf{x}_t|y)$ in each timestep is constantly associated with $\epsilon_\phi(\mathbf{x}_t, t, y)$. Hence, as Tang et al. [TWWZ23] have validated, by demonstrating the linear correlation between ϵ and $\nabla_{\mathbf{x}_t} \log p(\mathbf{x}_t|y)$, we can indirectly prove the timestep-dependent linear relationship between ϵ and $\epsilon_\phi(\mathbf{x}_t, t, y)$.

When $t = 0$, we prove that $\nabla_{\mathbf{x}_0} \log p(\mathbf{x}_0|y)$ is independent of ϵ . Since $x_0 = x + 0 \cdot \epsilon$, it is obvious that the inputs to $\nabla_{\mathbf{x}_0} \log p(\mathbf{x}_0|y)$ do not include any information about ϵ . Therefore, $\epsilon_\phi(\mathbf{x}_0, t, y)$ is purely unrelated to ϵ . When t increases to the upper limit t_{max} , we prove that $\nabla_{\mathbf{x}_{t_{max}}} \log p(\mathbf{x}_{t_{max}}|y)$ is collinear to ϵ as follows:

$$\begin{aligned}
 \nabla_{\mathbf{x}_{t_{max}}} \log p(\mathbf{x}_{t_{max}}|y) &= \nabla_{x_{t_{max}}} \log \mathcal{N}(x_{t_{max}}; 0, \mathcal{I}) \\
 &= \nabla_{x_{t_{max}}} \left(-\frac{1}{2} x_{t_{max}}^T x_{t_{max}} \right) \\
 &= -\frac{1}{2} \nabla_{x_{t_{max}}} x_{t_{max}}^T x_{t_{max}} \quad (20) \\
 &= -x_{t_{max}} \\
 &= -0 \cdot x - 1 \cdot \epsilon \\
 &= -\epsilon,
 \end{aligned}$$

where the superscript T represents the vector transpose operation.

7.2. More Visual Results

We provide additional visual results in Figures 13 and 14, illustrating DreamMapping’s capacity in text-guided generation tasks.

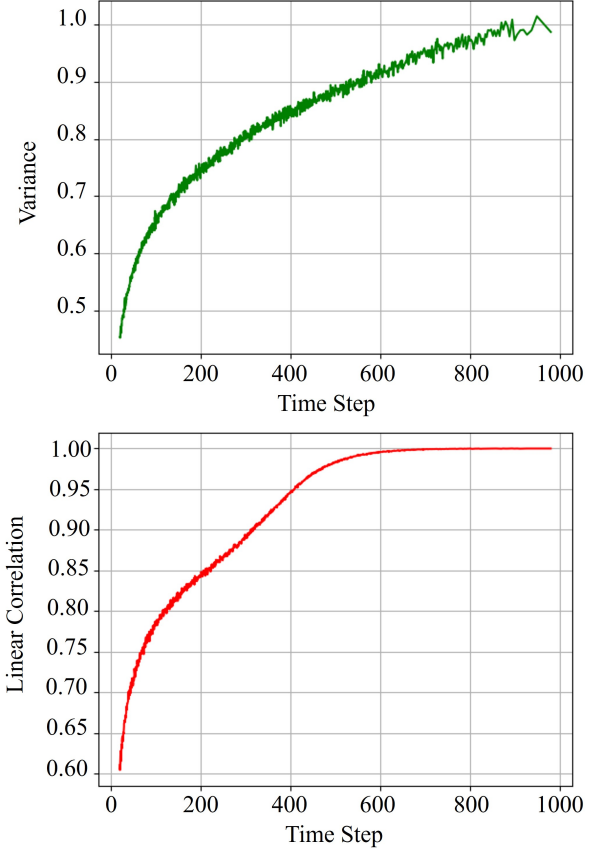


Figure 11: Variance of $\epsilon_\phi(\mathbf{x}_t, t, y)$ and linear correlation between ϵ and $\epsilon_\phi(\mathbf{x}_t, t, y)$ over time step t .

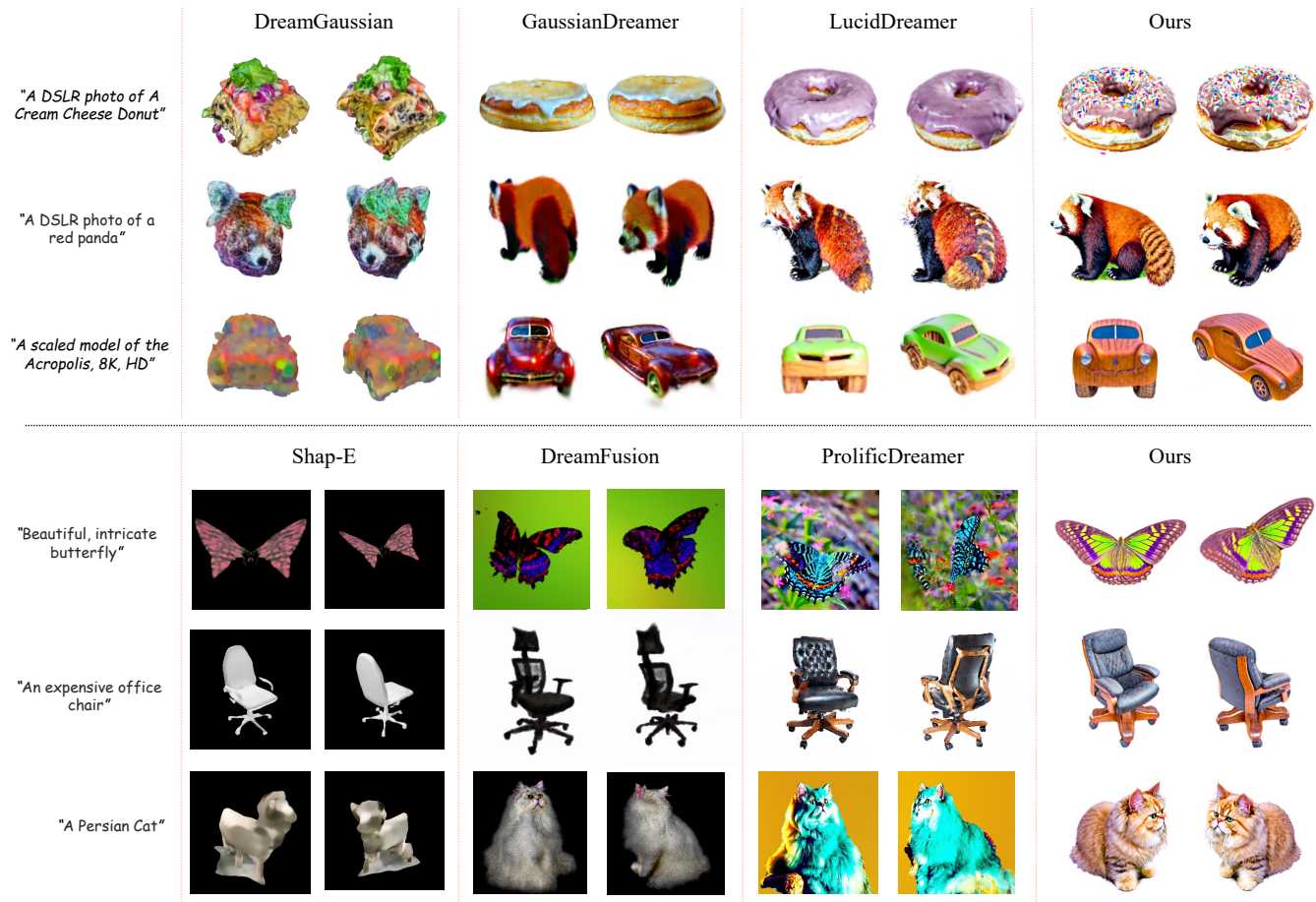


Figure 12: More qualitative comparisons with recent popular methods in text-to-3D generation. Please zoom in for details.



Figure 13: More text-to-3D results by our DreamMapping framework. Please zoom in for details.



Figure 14: More text-to-2D results using different base models, i.e., SD 2.1 Base [Stab] and DreamShaper V7 [Staa].